Check for updates

How to cite: *Angew. Chem. Int. Ed.* **2021**, *60*, 23444–23450
International Edition: doi.org/10.1002/anie.202109201
German Edition: doi.org/10.1002/ange.202109201

Oxygen Evolution

Single Particle Nanoelectrochemistry Reveals the Catalytic Oxygen Evolution Reaction Activity of Co_3O_4 Nanocubes

*Thomas Quast[+], Swapnil Varhade[+], Sascha Saddeler, Yen-Ting Chen, Corina Andronescu, Stephan Schulz, and Wolfgang Schuhmann**

Abstract: *Co_3O_4 nanocubes are evaluated concerning their intrinsic electrocatalytic activity towards the oxygen evolution reaction (OER) by means of single-entity electrochemistry. Scanning electrochemical cell microscopy (SECCM) provides data on the electrocatalytic OER activity from several individual measurement areas covering one Co_3O_4 nanocube of a comparatively high number of individual particles with sufficient statistical reproducibility. Single-particle-on-nanoelectrode measurements of Co_3O_4 nanocubes provide an accelerated stress test at highly alkaline conditions with current densities of up to 5.5 A cm^{-2}, and allows to derive TOF values of up to 2.8×10^4 s^{-1} at 1.92 V vs. RHE for surface Co atoms of a single cubic nanoparticle. Obtaining such high current densities combined with identical-location transmission electron microscopy allows monitoring the formation of an oxy(hydroxide) surface layer during electrocatalysis. Combining two independent single-entity electrochemistry techniques provides the basis for elucidating structure–activity relations of single electrocatalyst nanoparticles with well-defined surface structure.*

Introduction

Green energy storage becomes increasingly essential in the field of the provision of sustainable energy. Nanoparticle-based catalyst materials are comprised of a large number of individual particles, which exhibit a considerable variation in their individual size, shape, and surface structure.[1] Moreover, they are embedded in a catalyst layer comprising additives, leading to a high number of in-part dependent parameters, for example, the local change of the pH-value and other ensemble effects, which make the determination of intrinsic electrocatalytic and materials properties impossible. Single-entity electrochemistry (SEE) is employed to unravel intrinsic parameters of an electrochemical system down to individual electroactive sites.[2,3] Since electrodes with nanometric dimensions became accessible, several tools at the single-entity level were suggested, such as scanning electrochemical cell microscopy (SECCM),[4] nano-impact electrochemistry,[5,6] or the attachment of a specific nanoparticle to a nanoelectrode.[7] Their goal is to ultimately determine the intrinsic properties of materials during specific electrochemical reactions.[8] The attachment of a single nanoparticle onto a nanoelectrode is the crucial critical step and especially challenging to realize.[9] Recently, we reported a method to attach and investigate well-defined hexagonal-shaped single Co_3O_4 nanoparticles to the tip of a carbon-based nanoelectrode (CNE) using a robotic micromanipulator inside the scanning electron microscope (SEM).[10] SECCM has been employed for determining the structure–activity correlation of different electrochemically active surfaces and nanomaterials, offering a spatial resolution down to single nanoparticles.[11,12] Investigating the droplet landing areas of SECCM by means of SEM or TEM allows to derive structure–activity correlation.[12,13] All SEE techniques have their inherent benefits and drawbacks. On the one hand, SECCM offers a high statistical reliability concerning the intrinsic catalytic properties of nanoparticles or substrates due to the large number of independent measurements in a single SECCM scan. On the other hand, SECCM measurements in highly alkaline media, as typically used in industrial electrolyzers, are rather difficult due to surface wetting issues. Nano-impact measurements provide high statistical data and can be performed in high alkaline conditions. However, the duration of the impact and thus that of the electrochemical reaction is limited to a few milliseconds. Post-electrocatalysis characterization of structural changes, for example, by means of transmission electron microscopy (TEM), is impossible. Single particles attached to

[*] T. Quast,[+] S. Varhade,[+] Prof. Dr. W. Schuhmann
Analytical Chemistry—Center for Electrochemical Sciences (CES), Faculty of Chemistry and Biochemistry, Ruhr University Bochum
Universitätsstr. 150, 44780 Bochum (Germany)
E-mail: wolfgang.schuhmann@rub.de
Dr. S. Saddeler, Prof. Dr. S. Schulz
Inorganic Chemistry, Faculty of Chemistry and Center for Nanointegration (CENIDE), University of Duisburg-Essen
Universitätsstr. 7, 45141 Essen (Germany)
Dr. Y.-T. Chen
Center for Solvation Science (ZEMOS), Ruhr University Bochum
Universitätsstr. 150, 44801 Bochum (Germany)
Prof. Dr. C. Andronescu
Chemical Technology III, Faculty of Chemistry and Center for Nanointegration (CENIDE), University of Duisburg-Essen
Carl-Benz-Strasse 199, 47057 Duisburg (Germany)
[+] These authors contributed equally to this work.
Supporting information and the ORCID identification number(s) for the author(s) of this article can be found under: https://doi.org/10.1002/anie.202109201.

© 2021 The Authors. Angewandte Chemie International Edition published by Wiley-VCH GmbH. This is an open access article under the terms of the Creative Commons Attribution Non-Commercial NoDerivs License, which permits use and distribution in any medium, provided the original work is properly cited, the use is non-commercial and no modifications or adaptations are made.

the tip of a carbon nanoelectrode (CNE) can operate under high alkaline conditions and at high current densities, which offers the possibility to perform accelerated stress tests to induce structural changes. Moreover, the particle-at-the-stick methodology is designed to allow identical location TEM characterization of the nanoparticle before and after the electrochemical stress test. However, the method is limited in the number of possible measurements due to the challenges to place a single nanoparticle on the surface of a CNE. Therefore, we combine two SEE techniques to compensate for the inherent limitations of the particular methods and to gain a unique insight into the intrinsic structure–activity correlation of a single Co_3O_4 nanocube. Through the combination of SECCM with the single-particle-at-the-tip approach, on the one hand, a statistically relevant number of measurements of the intrinsic electrocatalytic OER activity of a single Co_3O_4 nanocube at low alkaline conditions becomes accessible. On the other hand, electrochemical and identical-location structural TEM data are obtained.

Here, we demonstrate that combining SECCM and the single-particle-at-the-tip approach, the intrinsic electrocatalytic activity and structural changes during an accelerated stress test of well-defined Co_3O_4 nanocubes concerning the OER can be assessed.

Results and Discussion

First, SECCM with subsequent SEM visualization of the droplet landing sites is used to obtain the voltammetric activity scans of a statistically significant number of single Co_3O_4 nanocubes to derive a first estimate of the OER turnover frequency (TOF). The TOF is a direct measure of the electrocatalytic turnover of an individual active site at the nanoparticle surface towards the OER. Unlike our previous study using Co_3O_4 hexagons,[9] the cubes are ideally exposing exclusively the (100) surface plane of the Co spinel and hence the TOF values represent the catalytic turnover of Co atoms at a single lattice plane. In the following step, we perform single-particle-at-the-tip measurements under the same conditions as used for the SECCM measurements (Scheme 1). Finally, a voltammetric scan is performed at the Co_3O_4 nanocube-modified CNE to an anodic potential of 1.9 V vs. RHE to achieve the highest possible current from the catalyst particle without deteriorating the integrity of the underlying carbon nanoelectrode. At these high current densities in highly alkaline electrolytes, the single catalyst particle experiences an accelerated stress test to elucidate the stability of the spinel-type Co_3O_4 cube at current densities far above those relevant for industrial applications. This provides the opportunity to investigate the same Co_3O_4 cube electrochemically, structurally and concerning its compositional changes imposed by the accelerated stress test employing TEM and EDX. The cube-shaped Co_3O_4 nanoparticles of varying sizes (80–360 nm), with an average size of 207 nm, were synthesized using a hydrothermal method in the absence of any structure-directing agents (details in Section 2, ESI, Figure S1–S5).[12] The corresponding XRD pattern were assigned to phase-pure Co_3O_4 devoid of any traces of crystalline secondary phases such as hydroxides, as demonstrated by the Rietveld refinement (Figure S1).

Nanopipettes for the SECCM measurements were pulled quartz capillaries with diameters between 400 to 500 nm (Figure S7) filled with 50 mM KOH solution, which contains 0.1 mM of an Os-complex [(Os (2,2′-bipyridine)$_2$(N,N′-dimethyl-2,2′-bisimidazole)] as free-diffusing redox mediator. A Pt wire with a diameter of 0.25 mm serves as quasi-reference/counter electrode. The Os-complex exhibits a pH-independent reversible Os^{3+}/Os^{2+} redox conversion which is used as a stable reference potential to convert the applied voltage to the RHE scale (details in Section 3, ESI).[11] The Co_3O_4 cubes were dispersed in toluene containing oleylamine using a tip sonicator for 15 min for improved particle separation (Figure S6). The well-dispersed solution was drop-coated onto a polished glassy carbon plate and subsequently heated for 2 h at 200 °C in an oven under ambient atmosphere to remove the oleylamine from the particle surface.[14] After installing the filled nanopipette and the glassy carbon plate with the Co_3O_4 nanocubes in the SECCM set-up (Figure S8), a hopping-mode SECCM scan was performed over an area of $100 \times 100\ \mu m^2$ with a hopping distance of 7 to 10 μm resulting in at least 100 measurements per scan and in total 2,300 landing sites. At each landing site of the nanodroplet, a series of cyclic voltammograms was recorded in a potential range from 0 to 0.6 V vs. Pt quasi-reference electrode. This potential range covers the Os^{3+}/Os^{2+} redox reaction. The obtained voltammograms were later used for the conversion of the potential to the RHE scale.

Afterwards, one linear sweep voltammogram (LSV) in the potential range from 0 to 0.9 V vs. Pt quasi-reference

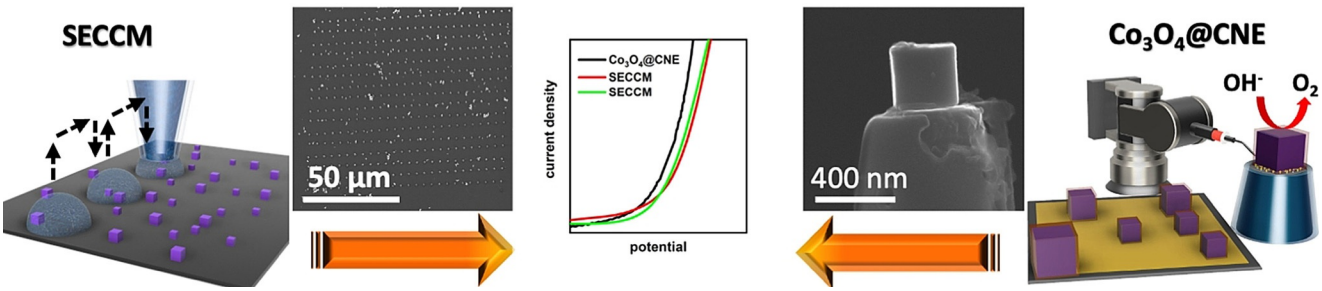

Scheme 1. Combination of SECCM and the particle-at-the-stick technique provides a unique approach to elucidate electrocatalytic properties as well as structural changes of individual Co_3O_4 spinel nanocubes.

 © 2021 The Authors. Angewandte Chemie International Edition published by Wiley-VCH GmbH

electrode was recorded at a scan rate of 1 $V s^{-1}$ to determine the OER activity of the individual site, which is wetted by the nanodroplet. Specific spots which showed higher current responses were analyzed with SEM to visualize the presence, the number and the size of the Co_3O_4 nanocubes at each individual measurement area. Approximately 80–100 landing sites with one or more Co_3O_4 nanocubes in the spot were investigated and 17 spots with one particle were selected. Among the single particle spots, only those spots had been finally selected which had perfect adjacent carbon measurements assuring the integrity of the capillary. From the size of the nanocube, the surface area and current density can be derived (Figure 1). The shown electrochemical response from a selection of those spots with a single particle was corrected by the baseline current obtained from adjacent bare carbon spots, which is the reason why the redox wave of the Os-complex is barely visible in the LSVs (Figure S9 and S10). All spots, which contain a single Co_3O_4 nanocube of varying size, show a very similar activity towards the OER when normalized to the geometric surface area (Figure 1). Table 1 lists the particle sizes and the respective calculated TOF values. The highest obtained current density at 1.9 V vs. RHE is 275 $mA cm^{-2}$, and the corresponding TOF value, which considers only the surface Co atoms assuming an exposed (100) surface plane (Figure S11), is $884 \pm 286\ s^{-1}$. The edge-length dependent TOF values are shown in Figure S12.

For cubes with an edge length exceeding approximately 300 nm, a decrease in the slope of the LSV is observed at higher anodic potentials resulting in a steady-state-like current response. This is attributed to the confinement in the nanodroplet and is likely due to the depletion of OH^- ions or O_2 saturation within the droplet. Limited diffusion of OH^- towards the catalyst particle or local oversaturation of O_2 impacts the reaction rate at high potentials.[14] Therefore, the single-particle-at-the-tip approach, which is not affected by a limited electrolyte volume in the direct vicinity of the single nanoparticle was applied to verify the results obtained from the SECCM measurements and extend them to higher current densities. Carbon nanoelectrodes were fabricated by pulling quartz glass capillaries with a laser puller and filling the nanometer-sized tips with carbon by pyrolysis as described previously.[15] The as-fabricated CNEs were further processed using focused ion beam (FIB) milling inside the SEM to obtain a disc-shaped electrode surface with a typical diameter of 300 to 500 nm (Figure S13). The surface of the FIB-processed CNEs was functionalized employing electrochemical oxidative grafting of N-BOC-ethylenediamine, yielding an amino-group functionalized surface after acid-cleavage of the BOC group (see ESI).[16] The functionalization is necessary to provide stronger interaction between the CNE surface and the Co_3O_4 nanocubes, which increases the chance that the particle sticks firmly on the surface. For the pick-up process of the single Co_3O_4 nanocube, the sample was dispersed in ethanol containing 0.03 vol. % of oleylamine for nanoparticle separation. The dispersion is sonicated and immediately drop-coated onto a flat gold-covered silicon wafer surface. Several CNEs, the gold wafer with the Co_3O_4 nanocubes, and the micromanipulator are installed in the SEM chamber for the placement process.

A single well-defined Co_3O_4 nanocube is selected under SEM control, picked up with the tip of the micromanipulator system, and placed onto the top of the CNE to obtain a Co_3O_4@CNE nanoassembly (Figure 2 a–d). The single-particle modified CNEs are heated to 200 °C for 2 h in air to remove the oleylamine from the nanoparticle surface.[14] Before the activated Co_3O_4@CNE nanoassembly was electro-

Table 1: Edge lengths of the Co_3O_4 nanocubes and corresponding calculated TOF values derived from the SECCM measurements shown in Figure 1.

Spot	Edge length [nm]	TOF @ 1.8 V vs. RHE [s^{-1}]	TOF @ 1.9 V vs. RHE [s^{-1}]
1	100	414	1396
2	175	232	1087
3	203	212	598
4	205	174	675
5	308	457	1019
6	310	404	901
7	313	223	531
8	331	349	863

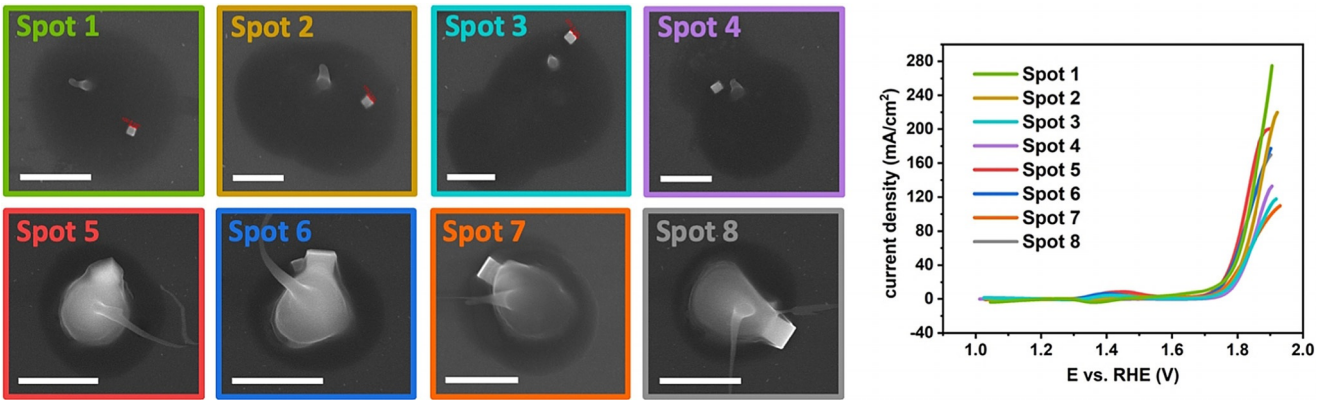

Figure 1. a) SEM images showing selected droplet-landing spots from a SECCM scan with a single Co_3O_4 spinel nanocube located within the droplet. The residues are due to dried KOH electrolyte. The scale bar equals 1 µm and the color code of the micrographs corresponds to that of the linear sweep voltammograms in b). Bare landing spot corrected linear sweep voltammograms recorded in 0.05 M KOH containing 0.1 mM Os-complex solution with a scan rate of 1 $V s^{-1}$.

 © 2021 The Authors. Angewandte Chemie International Edition published by Wiley-VCH GmbH

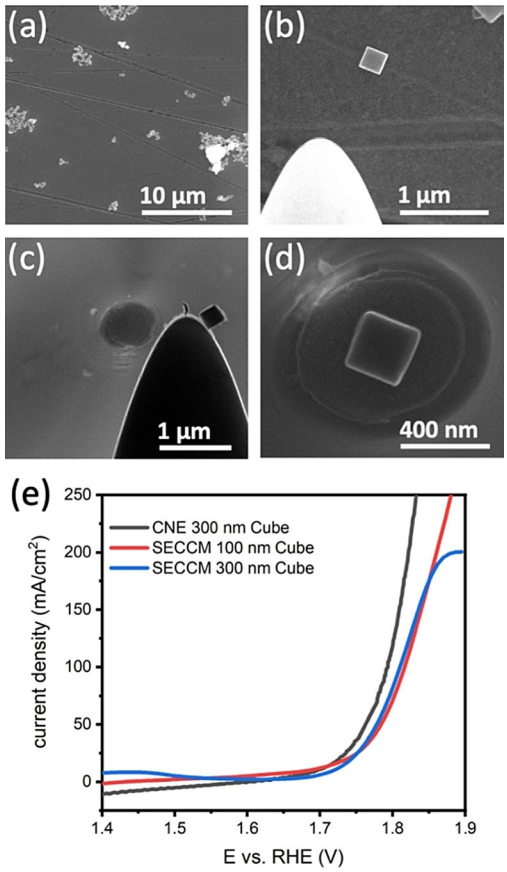

Figure 2. SEM images of a) Co_3O_4 nanocube particles drop-coated onto a gold-covered silicon wafer surface, b) a selected well-defined single Co_3O_4 nanocube particle with the tip of the micromanipulator tip in close proximity, c) a single Co_3O_4 nanocube particle attached to the micromanipulator tip close to the CNE surface, and d) a single Co_3O_4 nanocube particle placed on the CNE. Linear sweep voltammograms recorded from e) the single Co_3O_4@CNE nanoassembly (black) and by means of SECCM (green and red) with a scan rate of 1 $V s^{-1}$ in 0.05 M KOH containing 0.1 mM Os-complex.

chemically investigated, it was inspected by SEM to confirm that the nanocube is still firmly attached to the CNE surface. To compare the measurements between SECCM and the single-particle-at-the-tip approach, the same electrolyte was employed (0.05 M KOH containing 0.1 mM Os-complex). A LSV, which is corrected by the Os-complex redox current contribution (Figure S14), is shown in Figure 2 (dark grey) together with two LSVs obtained by single-particle SECCM measurements (red and blue). Both SEE approaches show similar results at lower current densities if the current was normalized to the surface area of the Co_3O_4 nanocube. The current density at 1.8 V vs. RHE is in average 81 mA cm^2 for the SECCM and 123 mA cm^2 for the Co_3O_4@CNE measurement, leading to TOF values of 414 s^{-1} for SECCM and 626 s^{-1} for the Co_3O_4@CNE experiment, respectively. With increasing overpotential for the OER, the difference in currents increases between both techniques, which is due to the restricted electrolyte volume and diffusional constraints in the SECCM configuration. A faster and unhindered diffusion of OH^- ions towards the Co_3O_4@CNE nanoassembly is the basis for long-term measurements and overall higher currents in the particle-at-the-stick approach (for details see ESI).

The benefit of the single-particle-at-the-tip approach lies in the possibility of a detailed structural characterization of the nanoassembly using TEM and TEM-EDS before and after the electrochemical experiments. To enable identical-location TEM with single nanoparticle-modified CNEs we designed a specific CNE-TEM holder (Figure S15). Due to the comparatively low current densities of approximately 1 A cm^2 and the short exposure time to high anodic potentials at the fast scan rate of 1 V s^{-1} no morphological changes at the particle surface were visible after the LSV sequence as also used in the SECCM measurements. TEM images show a homogeneous crystal lattice of the particle before and after the LSVs (Figure S16). Co_3O_4 nanocubes were investigated concerning their stability under conditions that are by far harsher than in industrial electrolyzers by performing accelerated stress tests at the level of a single catalyst particle. After fabrication of the nanoassembly by placing a single Co_3O_4 nanocube particle on a functionalized CNE surface, linear sweep voltammograms in 1 M KOH were performed at a scan rate of 200 mV s^{-1}. The achieved current densities of 5.5 A cm^{-2} under these conditions exceed industrial current densities (0.5 A cm^{-2}) by about ten times.[18] The same is true in comparison with the measurements performed in 0.05 M KOH. The calculated TOF values considering just the surface atoms at 1.9 V vs. RHE in 1 M KOH is 2.8×10^4 s^{-1} and thus several orders of magnitude higher than the ones reported above for 0.05 M KOH. If all Co atoms (surface and volume) of the nanoparticle are considered for TOF calculation, the TOF is lower than that reported for the hexagon-shaped Co_3O_4 particles.[8] However, normalized to the number of surface Co atoms in the Co_3O_4 nanocube considering (100) surface planes, the TOF value is in excellent agreement with that reported for hexagon-shaped Co_3O_4 particles ($2.7 \times 10^4 \pm 5 \times 10^3$ s^{-1}).[10] Ensemble measurements propose a trend that the activity towards the OER of the (100) lattice plane, which is present on the Co_3O_4 nanocube, has a lower activity than the (111) or (110) lattice planes, which are constituting the hexagon-shaped particles.[19] Due to the comparatively low number of Co atoms on the (100) plane, the current density of the Co_3O_4 nanocubes is roughly 5.5 A cm^{-2}, which is less than half of the current density that is obtained on hexagon-shaped Co_3O_4 particles (11.5 A cm^{-2}). The activity of the nanocubes is hence lower than the activity of the hexagon-shaped particles, if the current is normalized to the surface area, which agrees to ensemble measurements which were recently reported.[20] TEM analysis reveals significant changes in the particle morphology after the high-current density OER challenge of the single particle (Figure 3a,b). Prior to the electrochemical measurement, the distribution of Co and O was uniform across the whole particle, as shown by EDS analysis (Figure 4a–c). The nanoelectrode-attached Co_3O_4 nanocube is very homogeneous in terms of its element distribution before the accelerated stress test as demonstrated by the homogeneous contrast of the STEM image in Figure 4a and the EDS data shown in Figure 4b,c. The lattice fringes run through the particle as the whole (Figure S2).

 © 2021 The Authors. Angewandte Chemie International Edition published by Wiley-VCH GmbH

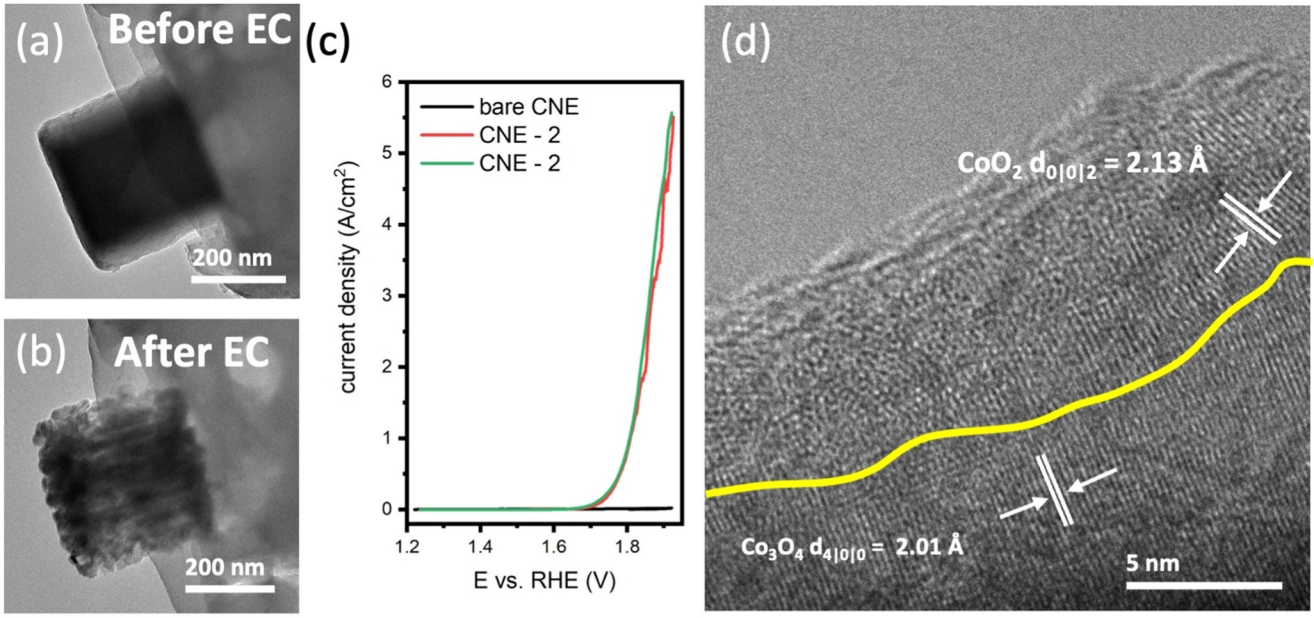

Figure 3. HR-TEM images of the same Co_3O_4 nanocube a) before and b) after the electrochemical stress test. c) Linear sweep voltammograms of two different Co_3O_4@CNE nano-assemblies and a bare carbon nanoelectrode (current density is normalized by their surface area). d) HR-TEM image of the near-surface region of the particle shown in b) (the yellow line indicates the near-surface amorphous region).

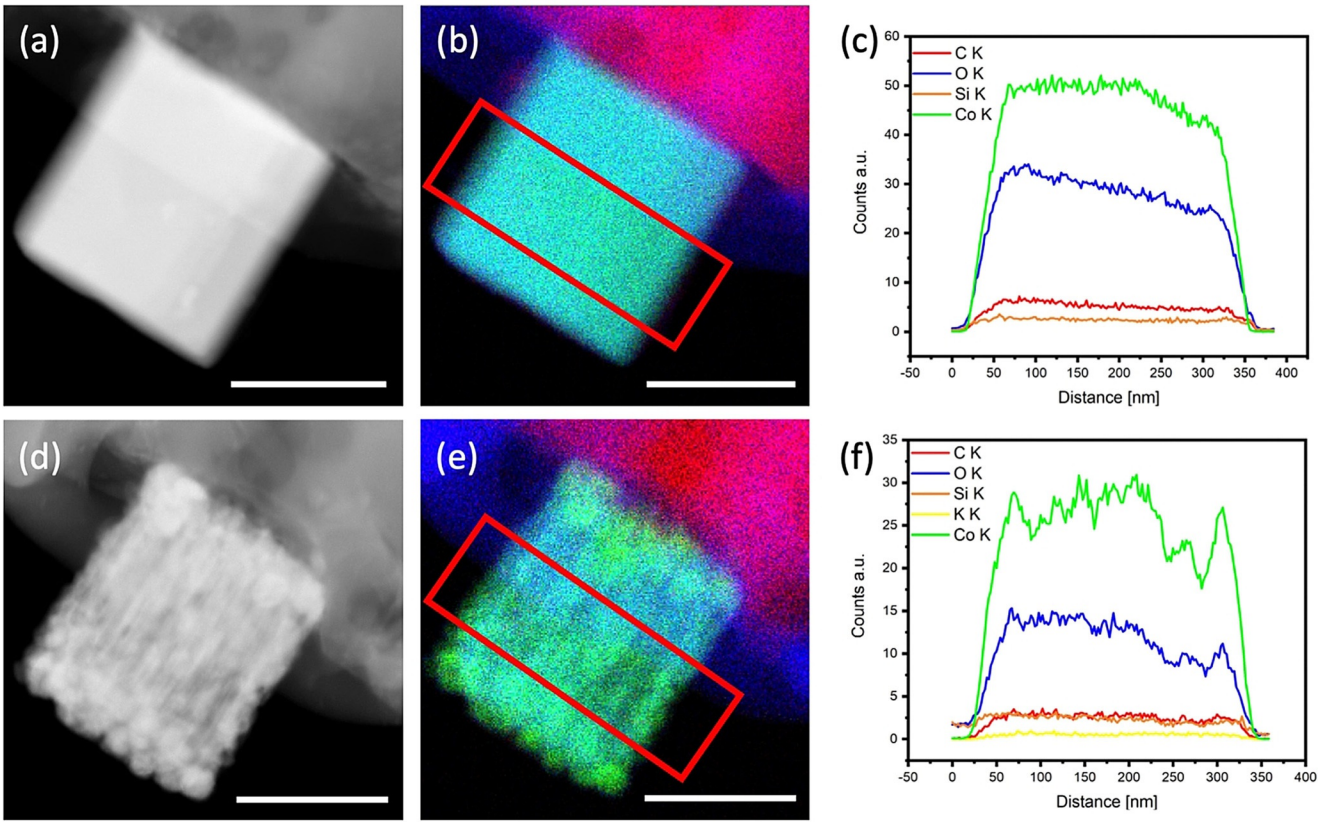

Figure 4. STEM micrographs of the same Co_3O_4@CNE nano-assemblies a) before and d) after the accelerated stress test. EDS analysis of the shown Co_3O_4@CNE nano-assemblies b) before and e) after the accelerated stress test. Line profile c) before and d) after the accelerated stress test obtained from the area marked with a red box in the corresponding EDS analysis. Scale bar is equal to 200 nm.

After the accelerated stress test, local agglomerations of Co_3O_4 are formed inside the particle which is losing its homogeneity. Especially the sharp edges of the nanocube disappeared during high current-density OER (Figure 3b and

 © 2021 The Authors. Angewandte Chemie International Edition published by Wiley-VCH GmbH

4) and concomitantly significant changes in the elemental distribution across the particle were observed by EDS analysis. The nanocube shows now regions with higher mass concentrations of Co (Figure 4d,e). The EDS analysis confirms that these denser areas consist of Co_3O_4 due to the direct correlation of the Co and O peaks in the line scan shown in Figure 4f obtained from the area marked in red in Figure 4e. Further structural changes become visible in the HR-TEM images (Figure 3b,d). In the inner part of the particle, the homogeneous lattice spacing of d = 2.04 Å (400) Co_3O_4 is still intact, but an amorphization of the surface of the particle occurs. Inside this mostly amorphous layer, small crystalline areas with lattice fringes of d = 2.18 Å are observed, which can be attributed to the lattice spacing of CoO_2 (002). Not only the surface was undergoing a significant morphological restructuration, but it also experienced oxidation and corrosive deterioration. This process is most likely due to the formation of a mixture of CoOOH, which is reported to be an amorphous gel-like structure and known to be the active species in the OER of Co_3O_4,[21] and CoO_2, which can form under these conditions.[22]

Conclusion

In summary, synthesis of shape-pure Co_3O_4 spinel nanocubes combined with single-entity electrochemistry techniques provide deeper insight into structure–activity relations during high current-density OER electrocatalysis. SECCM and single-particle-at-the-tip measurements yield comparable results, especially at comparatively low current densities. The data obtained by SECCM are suitable to determine size-activity and structure–activity correlations over a higher statistical number of experiments in the lower current density area. The single-particle-at-the-tip approach provides intrinsic activity data at high current densities and gives access to TOF values at high turnover ($2.8 \times 10^4\ s^{-1}$), which is in good agreement with our previous study ($2.6 \times 10^4\ s^{-1}$).[10] The determined TOF values are an order of magnitude lower than those reported for $CoFe_2O_4$ spinel particles shown recently.[5] However, most importantly the combination of several single-entity electrochemistry techniques such as SECCM and single particle at nanoelectrode assemblies pave the way for deciphering intrinsic electrocatalytic activity data, which provides a correlated understanding of structural transformations during electrochemical processes by combination with identical-location TEM investigations.

Acknowledgements

This research obtained funding from the Deutsche Forschungsgemeinschaft (DFG, German Research Foundation) within the collaborative research centre/transregio 247 "Heterogeneous Oxidation Catalysis in the Liquid Phase" TRR 247 [388390466] (projects A2 and C3) as well as under Germany's Excellence Strategy-EXC 2033-390677874-RESOLV. This project has received funding from the European Research Council (ERC) under the European Union's Horizon 2020 research and innovation programme (grant agreement CasCat [833408]). The mechanical workshop team at the faculty of chemistry and biochemistry, Ruhr University Bochum, is acknowledged for the contribution in designing and building the nanoelectrode TEM holder. We acknowledge Prof. Patrick Unwin from the University of Warwick for providing the initial control software (WEC-SPM) for our SECCM experiments. Open Access funding enabled and organized by Projekt DEAL.

Conflict of Interest

The authors declare no conflict of interest.

Keywords: carbon nanoelectrodes · Co_3O_4 nanocubes · electrocatalysis · SECCM · single-entity electrochemistry

[1] a) S. Cao, H. Huang, K. Shi, L. Wei, N. You, X. Fan, Z. Yang, W. Zhang, *Chem. Eng. J.* **2021**, *422*, 130123; b) S. Cao, N. You, L. Wei, C. Huang, X. Fan, K. Shi, Z. Yang, W. Zhang, *Inorg. Chem.* **2020**, *59*, 8522.
[2] L. A. Baker, *J. Am. Chem. Soc.* **2018**, *140*, 15549.
[3] Y. Wang, X. Shan, N. Tao, *Faraday Discuss.* **2016**, *193*, 9.
[4] N. Ebejer, M. Schnippering, A. W. Colburn, M. A. Edwards, P. R. Unwin, *Anal. Chem.* **2010**, *82*, 9141.
[5] A. El Arrassi, Z. Liu, M. V. Evers, N. Blanc, G. Bendt, S. Saddeler, D. Tetzlaff, D. Pohl, C. Damm, S. Schulz, K. Tschulik, *J. Am. Chem. Soc.* **2019**, *141*, 9197.
[6] a) W. Cheng, R. G. Compton, *TrAC Trends Anal. Chem.* **2014**, *58*, 79; b) E. N. Saw, V. Grasmik, C. Rurainsky, M. Epple, K. Tschulik, *Faraday Discuss.* **2016**, *193*, 327.
[7] a) J. Clausmeyer, J. Masa, E. Ventosa, D. Öhl, W. Schuhmann, *Chem. Commun.* **2016**, *52*, 2408; b) Y. Yu, Y. Gao, K. Hu, P.-Y. Blanchard, J.-M. Noël, T. Nareshkumar, K. L. Phani, G. Friedman, Y. Gogotsi, M. V. Mirkin, *ChemElectroChem* **2015**, *2*, 58.
[8] J. Clausmeyer, W. Schuhmann, *TrAC Trends Anal. Chem.* **2016**, *79*, 46.
[9] H. B. Aiyappa, P. Wilde, T. Quast, J. Masa, C. Andronescu, Y.-T. Chen, M. Muhler, R. A. Fischer, W. Schuhmann, *Angew. Chem. Int. Ed.* **2019**, *58*, 8927; *Angew. Chem.* **2019**, *131*, 9021.
[10] T. Quast, H. B. Aiyappa, S. Saddeler, P. Wilde, Y.-T. Chen, S. Schulz, W. Schuhmann, *Angew. Chem. Int. Ed.* **2021**, *60*, 3576; *Angew. Chem.* **2021**, *133*, 3619.
[11] a) J. T. Mefford, A. R. Akbashev, M. Kang, C. L. Bentley, W. E. Gent, H. D. Deng, D. H. Alsem, Y.-S. Yu, N. J. Salmon, D. A. Shapiro, P. R. Unwin, W. C. Chueh, *Nature* **2021**, *593*, 67; b) E. Daviddi, K. L. Gonos, A. W. Colburn, C. L. Bentley, P. R. Unwin, *Anal. Chem.* **2019**, *91*, 9229; c) Y. Takahashi, Y. Kobayashi, Z. Wang, Y. Ito, M. Ota, H. Ida, A. Kumatani, K. Miyazawa, T. Fujita, H. Shiku, Y. E. Korchev, Y. Miyata, T. Fukuma, M. Chen, T. Matsue, *Angew. Chem. Int. Ed.* **2020**, *59*, 3601; *Angew. Chem.* **2020**, *132*, 3629.
[12] T. Tarnev, H. B. Aiyappa, A. Botz, T. Erichsen, A. Ernst, C. Andronescu, W. Schuhmann, *Angew. Chem. Int. Ed.* **2019**, *58*, 14265; *Angew. Chem.* **2019**, *131*, 14403.
[13] M. Choi, N. P. Siepser, S. Jeong, Y. Wang, G. Jagdale, X. Ye, L. A. Baker, *Nano Lett.* **2020**, *20*, 1233.
[14] D. Li, C. Wang, D. Tripkovic, S. Sun, N. M. Markovic, V. R. Stamenkovic, *ACS Catal.* **2012**, *2*, 1358.
[15] M. E. Snowden, A. G. Güell, S. C. S. Lai, K. McKelvey, N. Ebejer, M. A. O'Connell, A. W. Colburn, P. R. Unwin, *Anal. Chem.* **2012**, *84*, 2483.

 © 2021 The Authors. Angewandte Chemie International Edition published by Wiley-VCH GmbH

[16] P. Wilde, T. Quast, H. B. Aiyappa, Y.-T. Chen, A. Botz, T. Tarnev, M. Marquitan, S. Feldhege, A. Lindner, C. Andronescu, W. Schuhmann, *ChemElectroChem* **2018**, *5*, 3083.
[17] M. Sosna, J.-M. Chrétien, J. D. Kilburn, P. N. Bartlett, *Phys. Chem. Chem. Phys.* **2010**, *12*, 10018.
[18] M. Carmo, D. L. Fritz, J. Mergel, D. Stolten, *Int. J. Hydrogen Energy* **2013**, *38*, 4901.
[19] Z. Chen, C. X. Kronawitter, B. E. Koel, *Phys. Chem. Chem. Phys.* **2015**, *17*, 29387.
[20] S. Saddeler, U. Hagemann, S. Schulz, *Inorg. Chem.* **2020**, *59*, 10013.
[21] a) A. Bergmann, E. Martinez-Moreno, D. Teschner, P. Chernev, M. Gliech, J. F. de Araújo, T. Reier, H. Dau, P. Strasser, *Nat. Commun.* **2015**, *6*, 8625; b) Y. Xu, F. Zhang, T. Sheng, T. Ye, D. Yi, Y. Yang, S. Liu, X. Wang, J. Yao, *J. Mater. Chem. A* **2019**, *7*, 23191.
[22] J. B. Gerken, J. G. McAlpin, J. Y. C. Chen, M. L. Rigsby, W. H. Casey, R. D. Britt, S. S. Stahl, *J. Am. Chem. Soc.* **2011**, *133*, 14431.

Manuscript received: July 10, 2021
Revised manuscript received: July 26, 2021
Accepted manuscript online: August 19, 2021
Version of record online: September 23, 2021

 © 2021 The Authors. Angewandte Chemie International Edition published by Wiley-VCH GmbH